SERI/TP--211-3967

DE91 002115

Research on Stable, High-Efficiency, Large-Area Amorphous Silicon Based Modules - Task B

Final Subcontract Report 1 March, 1989 - 28 February, 1990

K. W. Mitchell
D. R. Willet
Siemens Solar Industries
Camarillo, California

October 1990

SERI Technical Monitor: W. Luft

Prepared under Subcontract No. ZB-7-06003-3

Solar Energy Research Institute
A Division of Midwest Research Institute

1617 Cole Boulevard
Golden, Colorado 80401-3393

Prepared for the
U.S. Department of Energy
Contract No. DE-AC02-83CH10093

Printed in the United States of America
Available from:
National Technical Information Service
U.S. Department of Commerce
5285 Port Royal Road
Springfield, VA 22161

Price: Microfiche A01
Printed Copy A03

Codes are used for pricing all publications. The code is determined by the number of pages in the publication. Information pertaining to the pricing codes can be found in the current issue of the following publications which are generally available in most libraries: *Energy Research Abstracts (ERA)*; *Government Reports Announcements* and Index (*GRA* and I); *Scientific and Technical Abstract Reports (STAR)*; and publication NTIS-PR-360 available from NTIS at the above address.

SUMMARY

Objectives

The primary objective of this contract is to develop processes for the fabrication of stable, high-efficiency single-junction and tandem cells and modules based on thin film silicon:hydrogen alloys (TFS). The focus of the effort at Siemens Solar Industries, formerly ARCO Solar, Inc., is the development of a four-terminal hybrid tandem junction consisting of a copper indium diselenide (CIS) bottom circuit and a semitransparent TFS top circuit, which is illustrated in Fig. 1. The glass/glass package provides long term environmental durability. The front ZnO electrode to the TFS device allows both a gridless geometry, minimizing module shadowing losses, and an optical antireflection stack in conjunction with the front glass to promote optical coupling of the light into the module. For light that is transmitted through the TFS device, the back TFS ZnO electrode in conjunction with the clear optical polymer coupling layer (typically ethylene vinyl acetate) and the front ZnO electrode to the CIS minimize reflection (less than 4% due to these interfaces) and absorption losses and assist entry of the light into the CIS absorber layer.

The principal tasks of the project are to prepare and characterize TFS and CIS for uniform deposition over 900 cm^2, to investigate ohmic contacts, transparent conducting layers, and textured light trapping layers, and to develop and demonstrate thin film modules over 900 cm^2 with photostability. In Phase III of the project, a thin film module with 13% conversion efficiency over 900 cm^2 and

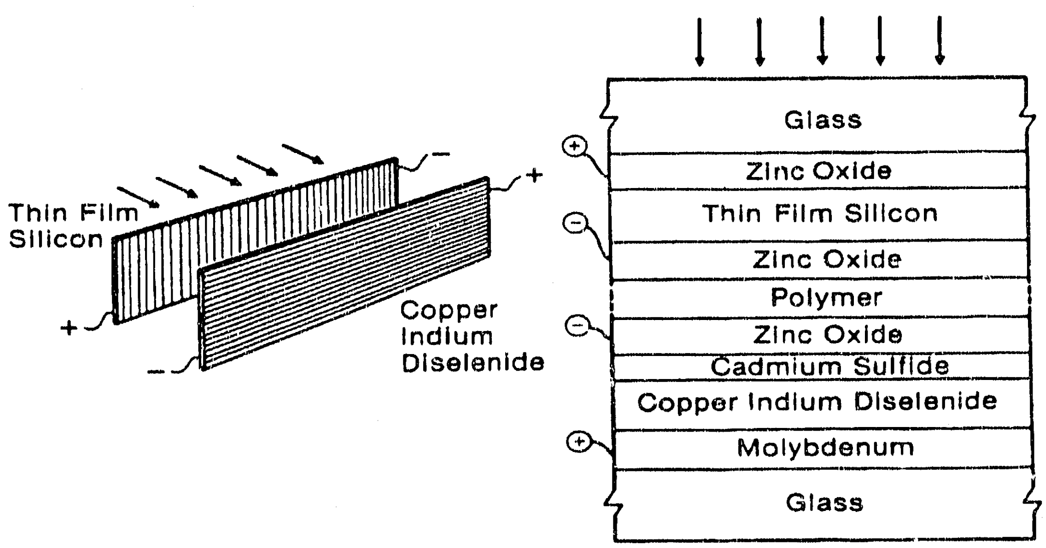

Fig. 1. TFS/CIS tander module structure.

photostability was to be demonstrated. However, due to lack of funds, the program was canceled at the end of Phase II. This report presents the technical progress for Phase IIB and represents the final technical report for the contract.

Discussion

Work during Phase I (July 1987 - August 1988) of this contract addressed development of the basic film deposition, junction formation, and patterning techniques necessary to fabricate high-efficiency cells and modules [1]. Module research during Phase IIA (September 1988 - February 1989) focused on transferring the technology to large areas (0.4 m^2) for both TFS and CIS. Film and junction uniformity have been tested on 4140 cm^2 substrates. CIS and semitransparent TFS modules with aperture areas near 3900 cm^2 have been developed [2]. Efforts during Phase IIB (March 1989 - February 1990) have been on the transfer of high efficiency thin film processing to the Siemens Solar facility in Camarillo, improving the performance of 0.4 m^2 thin film modules, developing large area tandem module packaging, and demonstrating 0.4 m^2, 4-terminal TFS/CIS laminated and framed thin film tandem modules.

The thin film single junction and tandem cell and module performance results achieved during the contract are summarized in Tables 1 through 5. During Phase I, a 15.6% active area efficient TFS/CIS tandem cell was demonstrated using a 10.3% semitransparent TFS and a 12.4% efficient CIS cell. In addition, a 12.3% aperture area efficient, 843 cm^2 4-terminal TFS/CIS module was measured using a 7.7% efficient semitransparent TFS module and a 7.6% efficient CIS module. The TFS-filtered CIS module contributed 2.7% efficiency to the tandem output, which is 35% of its stand-alone performance. The filtered CIS module output is primarily defined by its lower short-circuit current, which is 37% of its unfiltered value. During Phase I, a 3.5 cm^2, 14.1% active area efficient ZnO/thin CdS/CIS was also achieved with 41.0 mA/cm^2 J_{sc}, 508 mV V_{oc}, and 0.677 fill factor [1].

Emphasis during Phase II was on large area thin film module development, resulting in substantial performance achievements over large areas. A 33.2 watt (8.4% efficient), 3970 cm^2 aperture area TFS module with a white back reflector was demonstrated. Without the white back reflector, the semitransparent TFS module measured 30.2 watts or 7.6% efficient. Placing a laminated 31.6 watt, 8.1% efficient CIS module underneath this TFS module, with an air gap between the two modules, produced 11.2 watts or 2.9% over a 3883 cm^2 aperture area. Thus, the 4-terminal tandem power output is 41.4 watts, translating to 10.5% aperture efficiency. The TFS-filtered to unfiltered CIS power ratio of 0.35 is controlled by the current ratio of 0.38. Subsequently, a 37.8 watt (9.7% aperture efficiency) CIS module has also been demonstrated with a 3905 cm^2 aperture area.

Progress has been made on environmentally durable module packaging techniques. A glass/glass module lamination with a reaction injection mold (RIM) frame has been developed. A laminated TFS/CIS tandem module changed less than 14% after 576 days of continuous outdoor exposure. The CIS subcircuit showed no loss. Two laminated CIS modules are within 5% of their original output power after 470 days at the SERI outdoor photovoltaic test site.

Future performances of 3900 cm^2 aperture-area single-junction and tandem modules have been modeled, and module powers over 50 watts (13%) for CIS and over 65 watts (17%) for TFS/CIS tandems are predicted.

Conclusions

Film deposition and patterning processes have been successfully extended to 0.4 m^2 substrates. Large area module performance, which is presently in the 10% efficiency range, clearly confirms the scalability of thin film PV processing. TFS module stability, influenced both by Staebler-Wronski effects and by local defects, has been improved by careful process control and handling. CIS module stability is encouraging. Progress has been made on environmentally durable packaging for single-junction and tandem modules. Future performances of 3900 cm^2 aperture-area single-junction and tandem modules have been modeled, and module power over 50 watts (13%) for CIS and over 65 watts (17%) for TFS/CIS tandems are predicted.

Key achievements of the contract are summarized below:

- Achieved all objectives for uniform, large-area, high performance CIS and TFS semiconductor films.
- Developed large area deposition of doped ZnO films with resistivities as low as 5×10^{-4} Ω-cm and high optical quality.
- Developed modeling and analysis of TFS and CIS cells and modules to assess mechanisms controlling PV performance.
- Identified photocarrier recombination in the front *p-i* interface region as important to the suppression of V_{oc} and fill factor in TFS devices.
- Demonstrated a 10.8%, 3.9 cm^2 total area semitransparent TFS cell with no optical back reflector. This is equivalent to 11.9% efficiency for TFS cells with back optical reflectors.
- Developed thin film module patterning technology to achieve 254 μm interconnects, which results in only 5% active module area loss. This was achieved by improving registration of the interconnect scribes.

- Demonstrated that localized defects significantly influence TFS module performance and photostability.

- Identified and resolved several thin film module processing problems including substrate contamination, source material contamination, parts handling, and thin film deposition control.

- Accomplished several world performance records:

4 cm^2 TFS/CIS tandem cell	15.6%
4 cm^2 ZnO/thin CdS/CIS cell	14.1%
900 cm^2 TFS/CIS tandem module	12.3%
900 cm^2 CIS module	11.2%
900 cm^2 TFS module	9.4%

- Demonstrated excellent outdoor stability of encapsulated CIS modules (within 5% after more than 470 days).

- Demonstrated 10.4%, 840 cm^2 TFS/CIS tandem module with only 14% performance loss after 576 days of outdoor exposure. CIS subcircuit showed no loss.

- Explored large area (3900 cm^2) module processing with the following demonstrated aperture efficiencies:

3905 cm^2 unlaminated CIS	9.7% (37.8 W)
3883 cm^2 laminated CIS	8.7% (33.7 W)
3970 cm^2 back reflector TFS	8.4% (33.2 W)
3970 cm^2 semitransparent TFS	7.6% (30.2 W)
3883 cm^2 filtered CIS	2.9% (11.2 W)
TFS/CIS tandem module (air gap)	10.5% (41.4 W)

Table 1. 4-terminal tandem cell performance[a].

4 cm^2 Cell	Eff. (%)	J_{sc} (mA/cm^2)	V_{oc} (mV)	FF
Semitransparent TFS	10.3	16.4	871	0.72
Filtered CIS	5.3	17.9	432	0.68
Tandem	15.6			
Stand-Alone CIS	12.4	41.2	455	0.66

[a]Measured at ASTM air mass 1.5, global 100 mW/cm^2, 25°C.

Table 2. 1×1 ft tandem module performance[a].

30×30 cm Module	Power (W)	Area[b] (cm^2)	Eff. (%)	I_{sc} (mA)	V_{oc} (V)	FF
Semitransparent TFS	7.69	843	9.1	262	43.5	0.68
Filtered CIS	2.66	843	3.2	228	19.2	0.61
Tandem	10.35		12.3			
Stand-Alone CIS	7.62	844	9.0	611	21.2	0.59

[a]Measured at ASTM air mass 1.5, global 100 mW/cm^2, 25°C.
[b]Aperture area.

Table 3. 1×4 ft tandem module performance[a].

32×128 cm Module	Power (W)	Area[b] (cm^2)	Eff. (%)	I_{sc} (A)	V_{oc} (V)	FF
Semitransparent TFS	30.2	3970	7.6	1.03	47.2	0.62
Filtered CIS	11.2	3883	2.9	0.81	20.8	0.59
Tandem	41.4		10.5			
Stand-Alone CIS	31.6	3883	8.1	2.39	23.1	0.57

[a]Measured at ASTM air mass 1.5, global 100 mW/cm^2, 25°C.
[b]Aperture area.

Table 4. TFS and CIS cell performance[a].

	Area[b] (cm^2)	Eff. (%)	J_{sc} (mA/cm^2)	V_{oc} (mV)	FF
Semitransparent TFS	3.9	10.8	17.1	867	0.72
Stand-Alone CIS	3.5	14.1	41.0	508	0.68

[a]Measured at ASTM air mass 1.5, global 100 mW/cm^2, 25°C.
[b]Based on active area. For TFS, total area equals active area.

Table 5. TFS and CIS unlaminated module performance[a].

	Power (W)	Area[b] (cm^2)	Eff. (%)	I_{sc} (mA)	V_{oc} (V)	FF
Back Reflector TFS	7.9	844	9.4	277	42.8	0.67
	33.2	3970	8.4	1140	47.3	0.61
Semitransparent TFS	7.7	843	9.1	262	43.5	0.68
	30.2	3970	7.6	1030	47.1	0.62
Stand-Alone CIS	10.5	938	11.2	641	25.5	0.64
	37.8	3905	9.7	2510	23.9	0.63

[a]Measured at ASTM air mass 1.5, global 100 mW/cm^2, 25°C.
[b]Aperture area.

CONTENTS

Tables

CONTENTS
(continued)

Figures

SECTION 1.0

CIS PROGRESS

1.1 INTRODUCTION

During Phase IIB, the copper indium diselenide (CIS) fabrication activities were relocated to the Siemens Solar Camarillo facility. Unfortunately, permitting delays did not allow operation of the CIS facility until January 1990. This hindered our ability to fabricate CIS and thus 1×4 ft tandem modules of thin film silicon:-hydrogen alloy (TFS) over CIS. In spite of these delays, in initial operation at the upgraded Camarillo facility, the unencapsulated CIS module performance increased by 2 watts to 37.8 watts (9.7% aperture efficiency) over a 3905 cm^2 aperture area.

Maximum two-junction performance requires optimum high and low band gaps, which modeling has identified to be in the 1.7 eV and 1.0 eV ranges. CIS, a leading low band gap material, has demonstrated 14.1% (3.5 cm^2 active area) cell and 11.2% (938 cm^2 aperture area) and 9.7% (3905 cm^2 aperture area) module efficiencies [1,2]. The following sections describe the Phase IIB advancements in CIS large area modules, update results on long term outdoor exposure, and provide some perspectives on further advances in CIS modules. Finally, the potential for 20% efficient CIS device technology is discussed. With the appropriate high band gap module, this CIS technology will further enhance the potential of thin film tandem PV technology.

1.2 CIS MODULE PERFORMANCE

In Phase I, initial CIS module development was pursued on 1 ft^2 sizes, which resulted in 10.5 watts (11.2% aperture area efficiency) over a 938 cm^2 aperture area. The basic module design is described in previous reports [1,2]. During Phase IIA of this project, the processing technology developed on 900 cm^2 substrates was extended to 4140 cm^2 (128.6×32.2 cm) substrates to fabricate 3900 cm^2 aperture-area modules (Fig. 1-1). The 4140 cm^2 glass substrate size is used in standard crystalline silicon and TFS products. The CIS module is divided into 53 cells, each measuring 0.577 cm wide including interconnects. Approximately 240 cm^2 of the substrate perimeter area is used for electrical buses and for edge sealing pads. This perimeter area is subsequently covered by the module frame. The best large area CIS module performance achieved in Phase IIB was 35.8 watts (9.1% efficiency) over a 3916 cm^2 aperture area. After relocation of CIS processing to the Camarillo facility, initial operations have increased CIS module power by 2 watts to 37.8 watts (9.7% efficiency) over a 3905 cm^2 aperture area (Fig. 1-2).

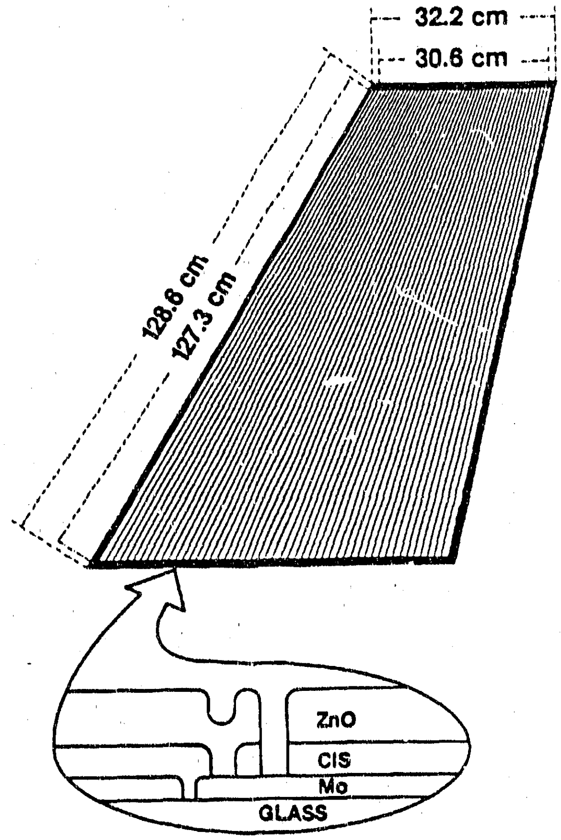

Fig. 1-1. Layout for 53-cell 1×4 ft CIS module.

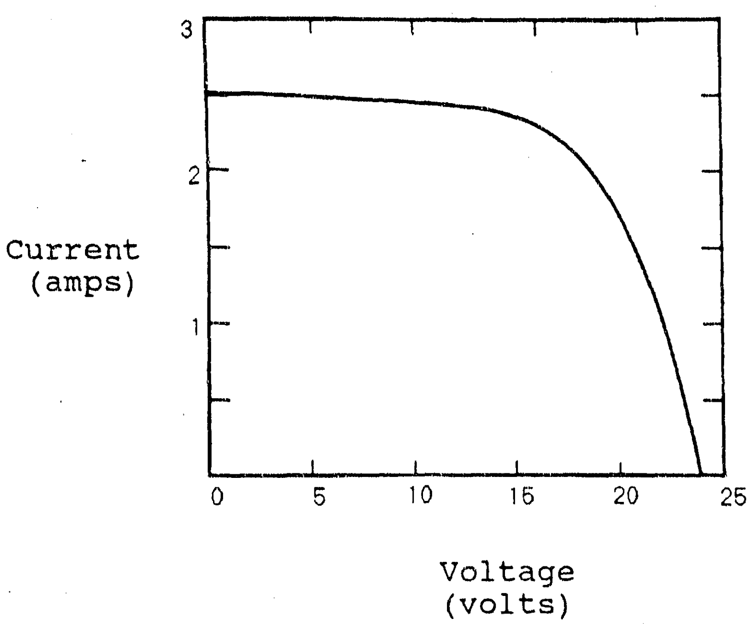

Aperture Area = 3905 cm^2
V_{oc} = 23.9 volts
I_{sc} = 2.51 amps
FF = 0.631
V_{max} = 17.7 volts
I_{max} = 2.13 amps
P_{max} = 37.8 watts

Fig. 1-2. Performance curve for 1×4 ft CIS module.

Table 1-1. Performance of CIS large area modules[a].

Module	Measurements 1×1 ft (55 cells)	Measurements 1×4 ft (53 cells)	Predictions 1×4 ft (53 cells)
Area[b] (cm^2)	938	3905	3900
V_{oc}/cell (mV)	464	451	508
J_{sc} (mA/cm^2)	39.3	36.6	41.0
V_{oc} (V)	25.5	23.9	26.9
I_{sc} (A)	0.641	2.51	2.86
Fill Factor	0.639	0.631	0.672
Eff[b] (%)	11.2	9.7	13.3
Power (W)	10.5	37.8	51.7

[a] 100 mW/cm^2 ASTM air mass 1.5 global spectrum, 25°C.
[b] Aperture area.

Table 1-1 compares the performance of the best 940 cm^2 and 3900 cm^2 modules fabricated to date. At present the interconnect widths on 3900 cm^2 modules are 0.041 cm compared to 0.025 cm for the best 940 cm^2 CIS module; therefore, the active area and I_{sc} are 3% lower than a linear extrapolation in aperture area predicts. Interconnect widths of 0.030 cm are expected to be achieved in the near future. The lower active area J_{sc}, V_{oc}/cell, and fill factor shown in the table for the 3900 cm^2 modules are the combined result of lower junction quality, lower ZnO uniformity, and pattern-induced shunting on the larger areas. When these problems are minimized, the aperture-area efficiency previously demonstrated on 940 cm^2 CIS modules will yield 43.6 watts on 3900 cm^2 module areas.

Future 3900 cm^2 CIS module performance has been modeled assuming the junction characteristics of the 14.1% efficient 3.5 cm^2 CIS cell previously reported, 0.030 cm interconnect widths, and the contact resistances typically measured on 940 cm^2 modules. The projection in Table 1-1 assumes that the module has uniform junction performance with 41 mA/cm^2 J_{sc}, 508 mV V_{oc}, 1.67 diode factor, 6 Ω/□ ZnO sheet resistance, and 0.001 Ω-cm^2 interconnect contact resistance. The model projects that the performance of 3900 cm^2 modules will be 51.7 watts (13.3% aperture efficiency) when the junction efficiency previously demonstrated on small-area cells is realized on the larger area.

1.3 CIS MODULE STABILITY

Module stability results are preliminary but are encouraging. Modules laminated with ethylene vinyl acetate (EVA) between a cover glass and a backing metal sheet show less than 5% change after more than 470 days of continuous exposure at the SERI outdoor test site

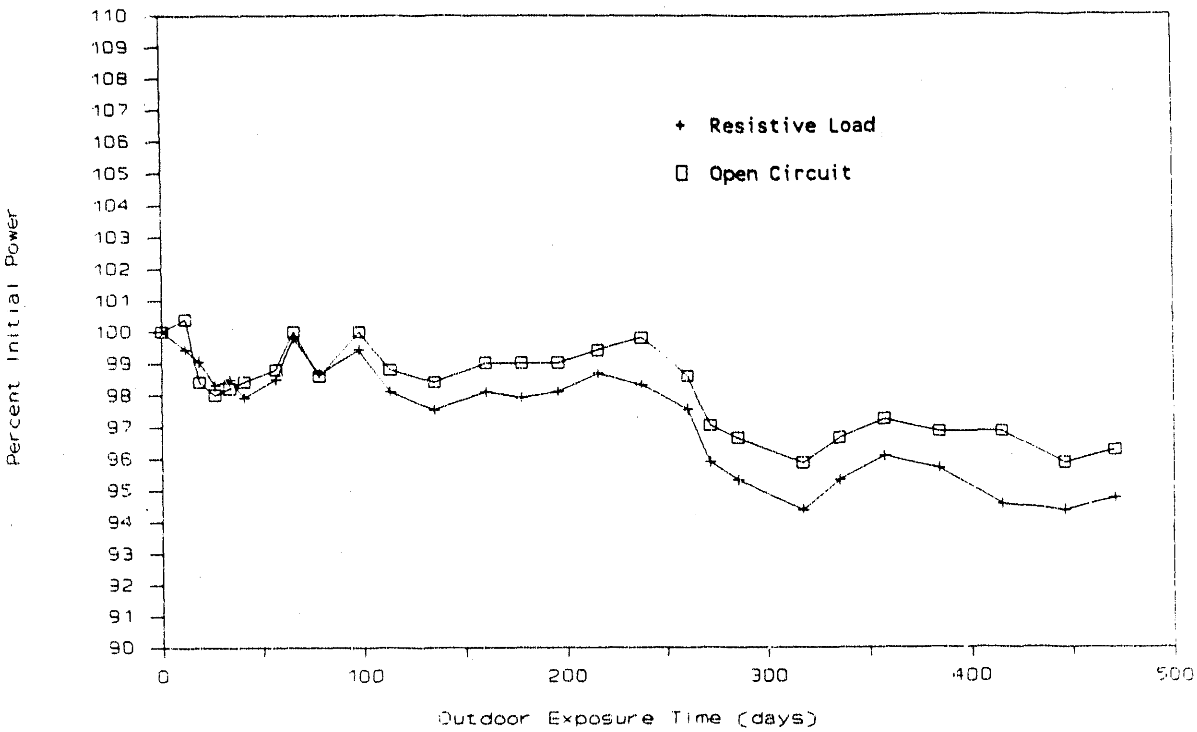

Fig. 1-3. Stability of CIS submodules after 470 days of outdoor exposure.

(Fig. 1-3) [3]. In production, the glass/glass CIS module laminate can be framed with a reaction injection molded (RIM) frame. A prototype glass/glass/RIM 3900 cm^2 module was measured at 33.75 watts at both SERI and Siemens Solar. Accelerated module life cycle testing indicates that further module packaging development is needed. Delamination between the top and bottom glass is evident for some modules. Reproducible edge sealing also needs improvements although excellent moisture sealing has been shown when the EVA cure level exceeds 90% in standard gel testing. The verification of CIS module stability is a major milestone in confirming the commercial viability of $CuInSe_2$ devices for high-power, low-cost PV applications.

1.4 TOWARD 20% CIS DEVICE TECHNOLOGY

This section addresses the efficiency limits of single-junction CIS-based alloy solar cells. CIS cell efficiencies of 20% and beyond are within reach with 45 mA/cm^2 J_{sc}, 600 mV V_{oc}, and 0.75 fill factor.

The highest CIS efficiency reported to date is 14.1%, achieved using the cell structure ZnO/thin CdS/CIS/Mo/glass [4]. The cell has a 41.0 mA/cm^2 J_{sc}, 508 mV V_{oc}, and 0.677 fill factor measured under 100 mW/cm^2 ASTM air mass 1.5 global spectrum [5].

Pursuit of high CIS efficiencies requires understanding the primary mechanisms controlling CIS device performance, especially photo-carrier collection, junction rectification, and electrical resistance losses. For 100 mW/cm^2 ASTM air mass 1.5 global spectrum, the theoretical maximum CIS photocurrent is 51 mA/cm^2, which is the number of photons with energy greater than the CIS band gap (assuming 0.95 eV). If all of these photons were absorbed by the CIS and made available to the external circuit at the CIS band gap energy, the efficiency would be dramatically high. Unfortunately, physical principles prohibit this. The following sections examine these physical principles, discuss measurements of device performance, and identify areas for improvement.

1.4.1 Photocurrent

Limitations to achieving 51 mA/cm^2 J_{sc} in CIS arise from optical reflection, unwanted optical absorption in front layers, incomplete optical absorption in the absorber layer, and incomplete minority carrier collection. For the 14.1% CIS cell, which has a 41.0 mA/cm^2 J_{sc}, the spectral response is described by

$$QE = (1-R) \times \exp[-\alpha_{ZnO} \times t_{ZnO}] \times \exp[-\alpha_{CdS} \times t_{CdS}] \times [1-\exp(-\alpha_{CIS} \times W_{CIS})/(1 + \alpha_{CIS} \times L_{CIS})] \quad \text{Eq. 1}$$

where R is the front reflection loss, α is the optical absorption coefficient [6] and t is the thickness of the respective layers, W is the depletion width, and L is the minority carrier diffusion length. Typical values are 0.4 µm for W and 0.5 µm for L. ZnO plasma absorption, evident at wavelengths longer than 900 nm, reduces J_{sc} by about 1 mA/cm^2, depending on the ZnO electron concentration and carrier mobility [4].

Improved ZnO front transparent electrode texture and conductivity will reduce optical reflection and plasma absorption losses, enhancing J_{sc} by 1.5 mA/cm^2 to 42.5 mA/cm^2. Optical confinement by reducing the CIS absorber thickness and using optical back reflectors will promote absorption of light in the active device region. In addition, improved minority carrier lifetime and/or the use of minority carrier mirrors will increase long wavelength (greater than 900 nm) response of the cell.

1.4.2 Open-Circuit Voltage

The achievement of 508 mV V_{oc} is a result of reducing the CIS reverse saturation current. The CIS current-voltage dependence on temperature implies that the dominant junction loss mechanism is recombination [7]. Microshunts (microscopic local areas of increased junction shunting) have been identified by optical-beam-induced current (OBIC) and electron-beam-induced current (EBIC) imaging [8,9]. Substantial spatial variations in electronic response up to 0.1 mm in size are also evident in these films.

Transmission electron microscopy (TEM) and energy dispersive X-ray analysis (EDX) have identified compositional and structural non-uniformities in the CIS layers [10]. In addition, intragrain and grain surface properties and both the CdS/CIS and Mo/CIS interfaces contribute to junction recombination. The CIS defect chemistry within the grains, at the grain surfaces, and at the junction and contact interfaces ultimately determines the limit to recombination. All of these are related to the processing of the device, either through the quality of the feedstock materials or through the processing conditions.

The additions of alloy elements, such as Ga and S, can also increase V_{oc} by increasing the absorber layer band gap as long as the minority carrier lifetime is not degraded. The nature of the heterojunction window layer also significantly impacts the V_{oc} and cell performance. High band gap II-VI and chalcopyrite window layers are options. Replacing CdS with thin ZnSe has already shown promise in preliminary studies, giving 10% efficiency, 40.1 mA/cm^2 J_{sc}, 391 mV V_{oc}, and 0.641 fill factor [11].

Continued optimization of processing conditions is expected to achieve 550 to 570 mV V_{oc}. Modifications to the material and interfaces will achieve V_{oc} of 600 mV and higher.

1.4.3 Fill Factor

The CIS fill factor is determined by the cell V_{oc} and the electrical resistance losses. Measurements of the fill factor dependence on cell geometry, light intensity, and temperature for the 12% CIS cell structure have been described elsewhere [7]. For the 14.1% CIS cell, its 0.677 fill factor will increase to 0.723 by reducing series resistance, primarily caused by the 13 Ω/□ front ZnO layer. Increasing the cell V_{oc} to 525, 550, 575, and 600 mV will increase fill factor to 0.729, 0.737, 0.744, and 0.751 respectively.

1.4.4 Conclusions

The practical limits to efficiency are the structural and electronic quality of the device layers and their interfaces, which are controlled by the processes used to form them. CIS cell efficiencies of 20% and beyond are within reach with 45 mA/cm^2 J_{sc}, 600 mV V_{oc}, and 0.75 fill factor.

1.5 DISCUSSION

During Phase IIB, the CIS fabrication activities were relocated to the Siemens Solar Camarillo facility. Unfortunately, permitting delays did not allow operation of the CIS facility until January 1990. This hindered our ability to fabricate CIS and thus 1×4 ft TFS/CIS tandem modules. In spite of these delays, in initial operation at the upgraded Camarillo facility, the unencapsulated

CIS module performance increased by 2 watts to 37.8 watts (9.7% aperture efficiency) over a 3905 cm^2 aperture area. Table 1-1 lists the performance parameters for the 37.8 W CIS module. The 35.8 W CIS module described in the previous report [2] had a 23.5 V V_{oc}, 2.54 A I_{sc}, and a 0.60 fill factor. Thus, the 5% increase in module power resulted primarily from a 5% improvement in fill factor (from 0.60 to 0.63) due to reduced series and shunt resistance losses. Although detailed analysis of the resistance mechanisms would require destructive testing of the module, the improved fill factor is expected to result from new patterning equipment developed outside of this contract which allows the interconnects to be scribed in one step. The previous patterning equipment required a step-and-repeat sequence to cover the 127 cm length of the interconnects in four steps.

High efficiency tandem PV modules depend upon the necessary contributions from the high and low band gap module components. CIS has been demonstrated to be an important low band gap cell technology with 14.1% measured active area efficiency and the potential of over 20% efficiency. More significantly, it is a proven module technology that has been scaled quickly to 37.8 watts (9.7% aperture efficiency). Modeling, based upon demonstrated technology, projects efficiencies in the 13% range, giving 52 watts over 3900 cm^2 aperture areas. As described above, several research tasks remain to optimize its cell and module performance as a single or tandem junction technology.

SECTION 2.0

TFS PROGRESS

2.1 INTRODUCTION

Activities related to thin film silicon:hydrogen alloy (TFS) focused on exploring large area (0.4 m^2) thin film processing during Phase IIB. During this period, in order to reduce sources of electrical shunts, a variety of process control advances were established including acid washing of glass, air-borne particulate control, glass edging, better front ZnO uniformity and optimizing laser parameters for the front ZnO cell isolation. The film qualities of devices made at the Camarillo facility were shown to be close to those made in the Chatsworth research lab.

2.2 TFS DEVICE STRUCTURE

The basic device structure of both semitransparent TFS cells and modules is glass/ZnO/*(graded dopant SiC p)-i-(graded dopant n)* TFS/ZnO [1-4]. The *p-i-n* TFS layers are deposited using a plasma discharge process. Tables 2-1 through 2-4 describe the TFS layer compositions and thicknesses, typical TFS deposition conditions, TFS layer properties, and ZnO properties. As discussed below, these material properties result in state-of-the-art high efficiency devices. For example, *p*- and *n*-layer conductivities of 2.6×10^{-5} and 3.5×10^{-2} respectively have been achieved [1]. No further optimization of the *p*- and *n*-layers was pursued during this period since the TFS cell efficiency presently is controlled more by the nature of the ZnO, the *i*-layer thickness, and by electrical shunting.

During Phase IIB, the measured performance of semitransparent TFS test structures improved to 10.8% efficiency (17.1 mA/cm^2 J_{sc}, 867 mV V_{oc}, 0.72 fill factor, 3.9 cm^2 active and total area) as shown in Fig. 2-1. This is due mainly to improved light trapping from the front ZnO. Previous analysis indicates that the I_{sc} and efficiency increase by 10% if a back optical reflector is incorporated. Thus, the 10.8% efficiency for the semitransparent TFS cell is equivalent to a 11.9% for a TFS device using a back optical reflector. As will be described in Section 2.3, identification and removal of debris and contamination that shunt the TFS junctions has been the major focus of efforts to improve cell and module performance.

The large-area TFS module consists of 54 series-connected cells with printed and fired silver paste buses near the edge of the glass (Fig. 2-2). The fabrication sequence for TFS modules, shown in Fig. 2-3, is similar to that for test cells except for the patterning steps. The busbar contacts in the cells and modules are

Table 2-1. TFS cell *p/i/n* layers.

Layer	Composition	Thickness
Front ZnO		1.3 μm
p-layer	graded Si:C:H alloy doped with B	0.010 μm
i-layer	standard, undoped Si:H alloy	0.345 μm
n-layer	microcrystalline Si:H alloy doped with P	0.030 μm
Back ZnO		1.3 μm

Table 2-2. TFS deposition conditions; experimental RF glow discharge reactor.

Layer	*p*	*i*	*n*
T(substrate), °C	205	205	205
p(total), torr	0.25	0.20	1.5
Power Density, mW/cm^2	9.5	8.5	87.0
Q(SiH_4), sccm	80	100	12
Q(H_2), sccm	0	0	500
Q(CH_4), sccm	35	0	0
Q(B_2H_6), sccm	32	0	0
Q(PH_3), sccm	0	0	3
Q(total), sccm	150	100	515
Turn-over Time, sec	5	7	10
Reactor Volume 52 liters			
Platen Area 1265 cm^2			

Table 2-3. TFS layer properties.

Layer	Eg (eV)	σ $(\Omega\text{-cm})^{-1}$	Ea (eV)
p-layer, standard	1.97	2.6×10^{-5}	
p-layer, microcrystalline	2.35	15	
n-layer, microcrystalline	1.7	0.035	0.14
i-layer, standard	1.74	5×10^{-9}	0.74 (dark)

Table 2-4. Zinc oxide layer properties.

Property	Value
Sheet rho	8-10 Ω/□
Resistivity	1.5×10^{-3} Ω-cm
Carrier concentration, n_e	1.0×10^{20} carriers/cm^3
Mobility, µm	35 cm^2/V-sec
Transmittance, 0.3-0.9 µm	80-85%

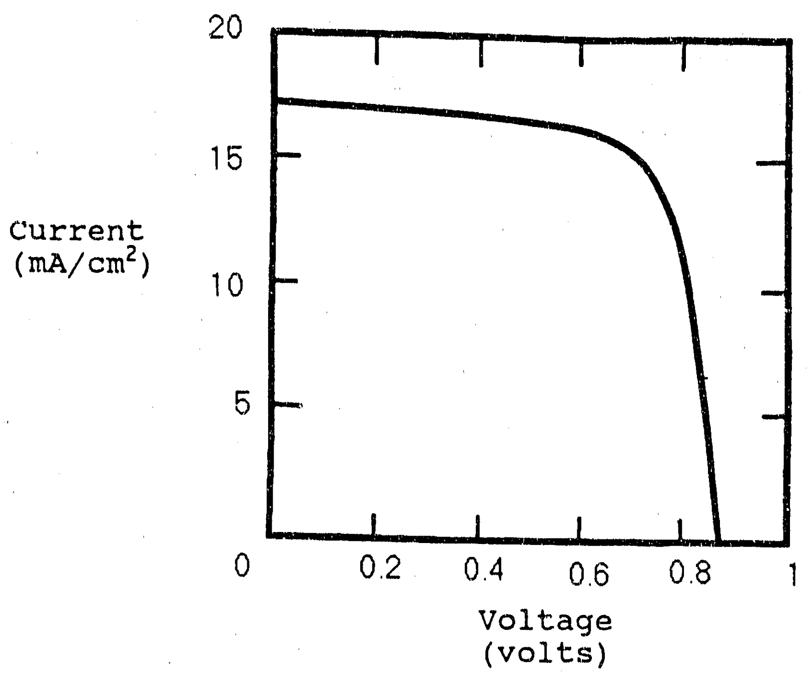

Cell Area = 3.9 cm^2
J_{sc} = 17.14 mA/cm^2
V_{oc} = 867 mV
J_{pm} = 15.13 mA/cm2
V_{pm} = 711 mV
FF = 0.724
Eff = 10.8%

Fig. 2-1. Best semitransparent TFS cell fabricated in Camarillo.

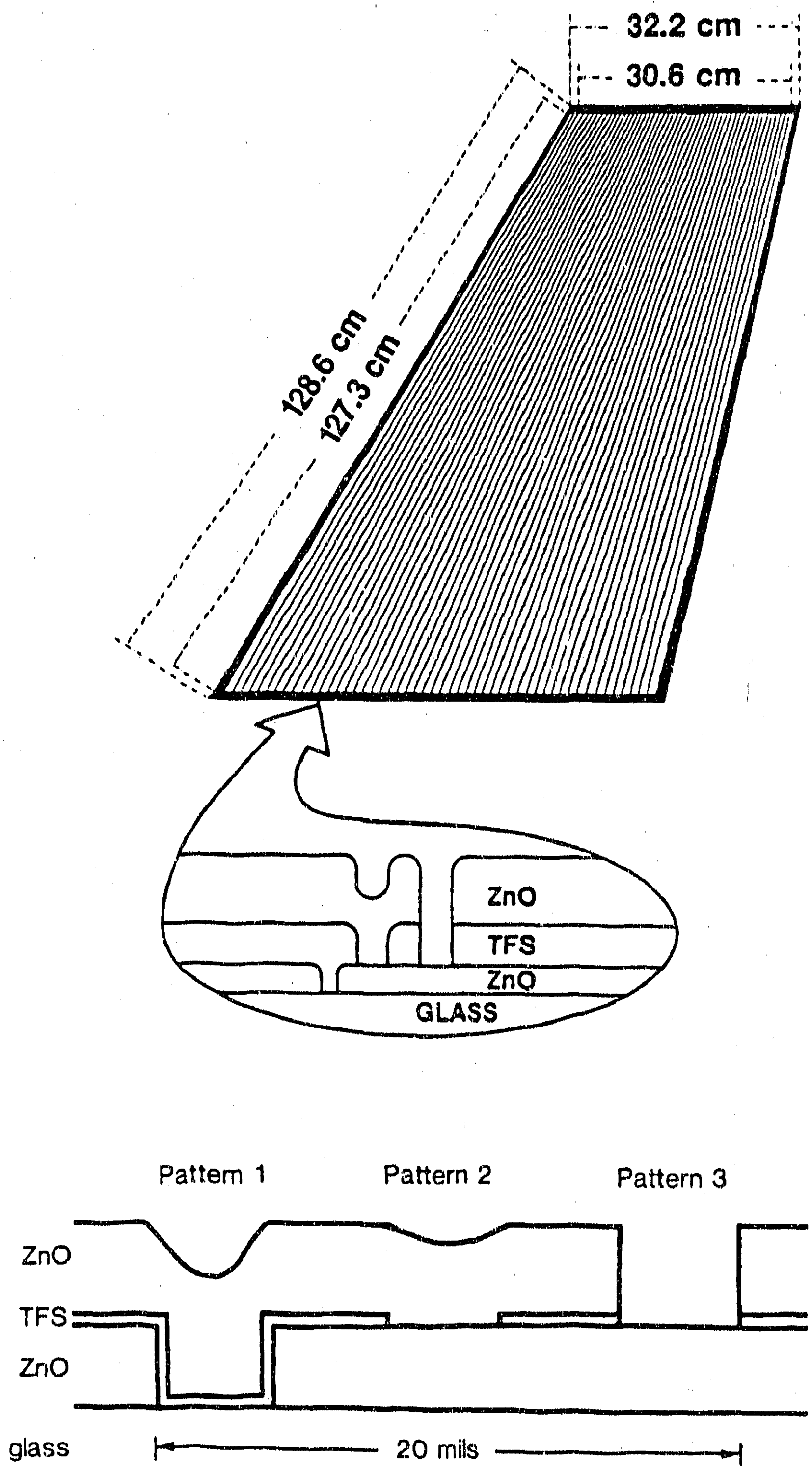

Fig. 2-2. Large area TFS module layout and interconnect structure.

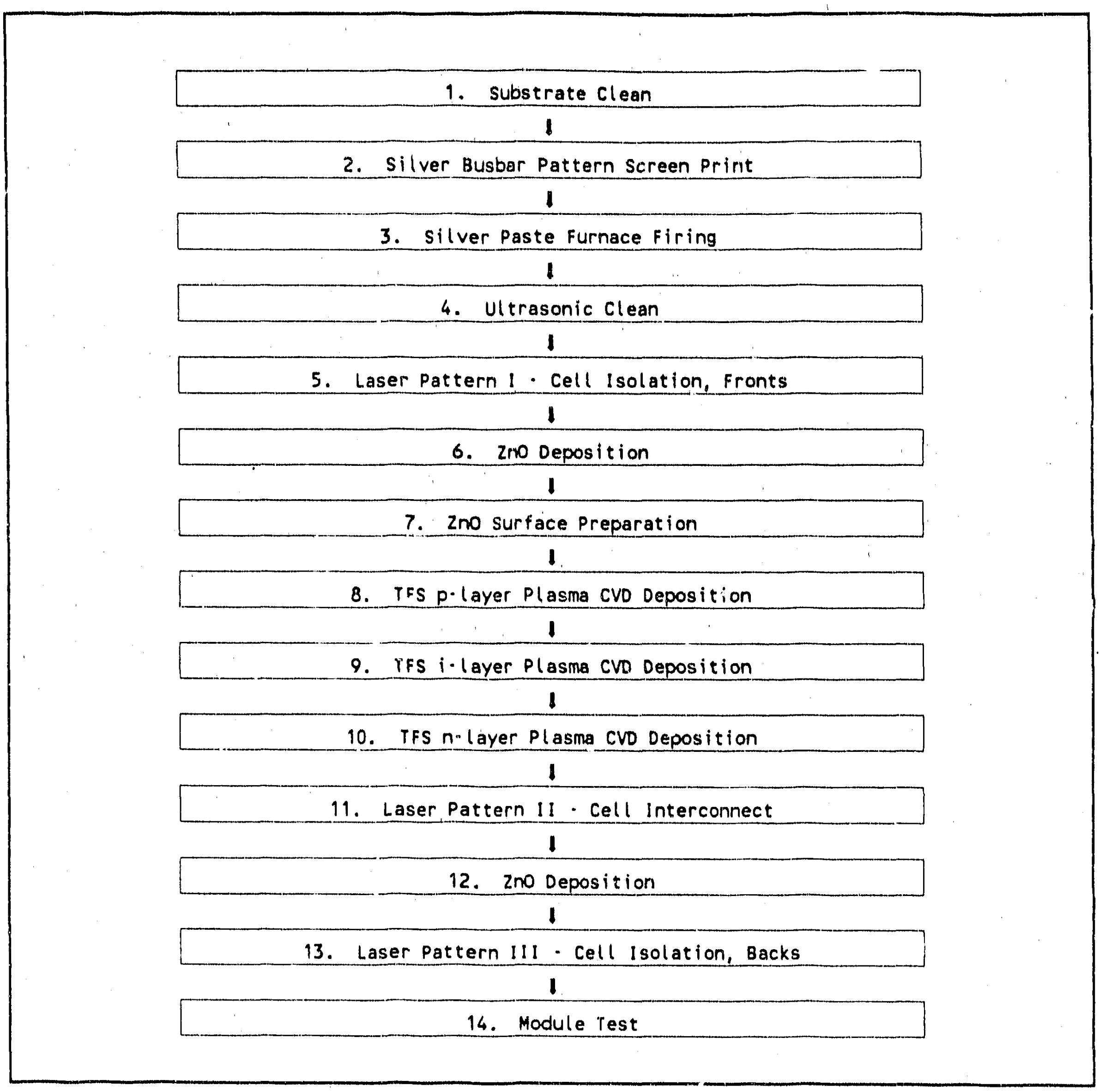

Fig. 2-3. TFS module fabrication sequence.

formed by firing a screen printed silver paste onto the glass substrate. Because the firing temperatures are above 400°C, the conductor adhesion to glass is higher than the cohesive strength of the glass. The contact of the silver to zinc oxide is ohmic and stable. No evidence of instability or degradation has been found at this contact interface. The device performance uniformity for 1×4 ft TFS modules is mapped using a 3×12 array of 10×10 cm test structures that contain 2 rows of 8 cells each.

2.3 TFS PROCESSING PROGRESS

During the fourth quarter of 1988, all TFS activities were transferred to the Camarillo facility. The transfer revealed device performance sensitivities that required a variety of process control improvements. For example, semitransparent TFS devices are sensitive to debris and contamination that shunt the junctions. Shunts can be caused by laser patterning debris, dirty substrates, static charge, and particulate contamination. Thus, substrate cleanliness is critical to assure TFS process reliability.

In Phase IIA, incoming glass was found to have "water marks" of unknown composition that caused areas of unusual ZnO growth. Studies found that water marks and their effects could be removed by pre-washing the glass substrates in acidic solutions (pH=3) [2].

A second problem identified was static charge build-up on bare glass prior to transparent conductor deposition. The charged glass attracts particulates. Small glass shards on the glass substrate are of particular concern. These shards subsequently bond to the substrate during heating and shunt the TFS module. Using a pencil edger and then giving a thorough cleaning immediately after the edging process was found to control glass shards. The pencil edger uses a wet diamond wheel to grind a smooth radius edge. Figure 2-4 shows the improved cell yields using pencil edgers compared to v-belt edgers for a 16-cell test structure.

Other airborne particulates can also cause shunts in TFS junctions. Ionizing nitrogen guns and pulsed antistatic bars have been installed on processing equipment to reduce particulate contamination. Downflow hoods and plastic curtains have also been installed at most process steps that take place before TFS deposition. Figure 2-5 identifies the particle counts at different processing stations under three conditions: (a) before installation of downflow hoods or curtains, (b) during production, and (c) when there is no activity. As shown, the quiescent particle counts are substantially reduced by the downflow hoods and other upgrades, but the particle counts increase during actual processing. The P1 area where the front ZnO is scribed remains to be upgraded.

The importance of TFS device shunting is evident in both the initial performance and in the outdoor exposure stability. The loss of module power with exposure is larger for lower initial shunt resistances. As shown in Fig. 2-6, devices with low initial resistances (less than about 1000 Ω-cm^2) degrade by up to 35% after a month of outdoor exposure compared to less shunted devices, which changed 20% or less. Almost all of the performance loss occurs in the first two weeks.

Module shunting was found to be the dominant power loss mechanism and thus was addressed first. Once the module shunt resistance is acceptably high, other loss mechanisms such as the Staebler-Wronski

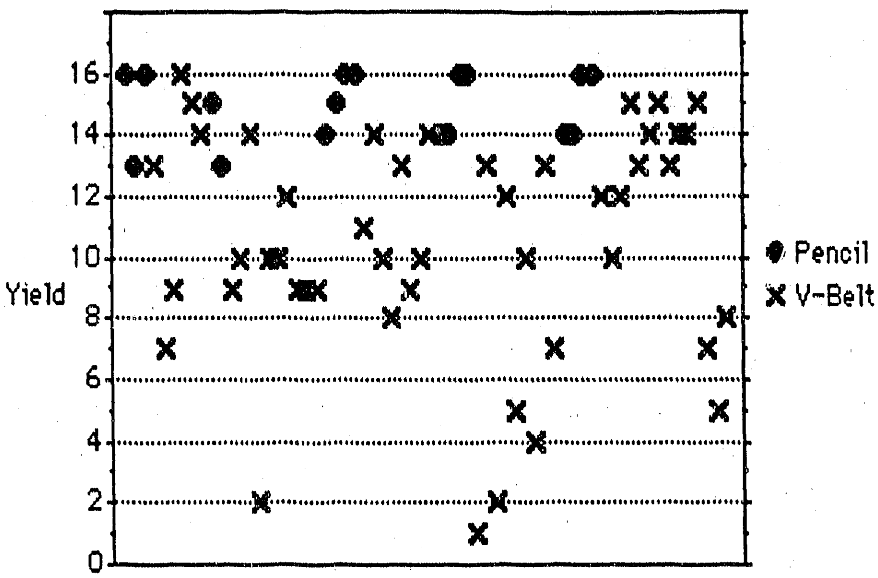

Fig. 2-4. Effect of pencil versus v-belt edger on yield of good TFS cells.

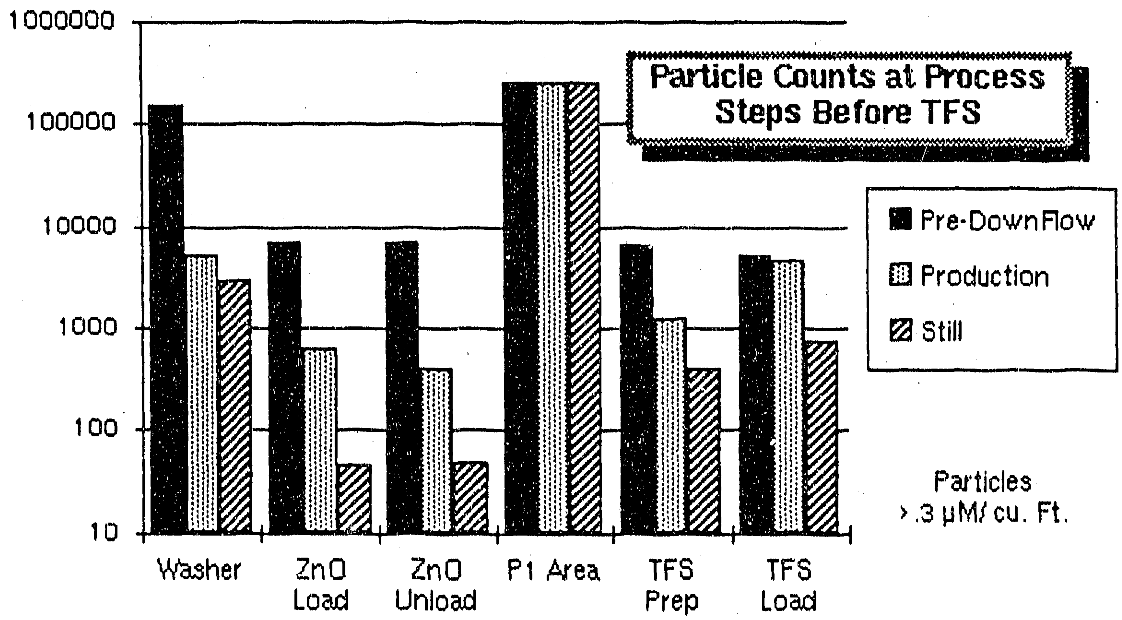

Fig. 2-5. Airborne particulate counts at various TFS process steps.

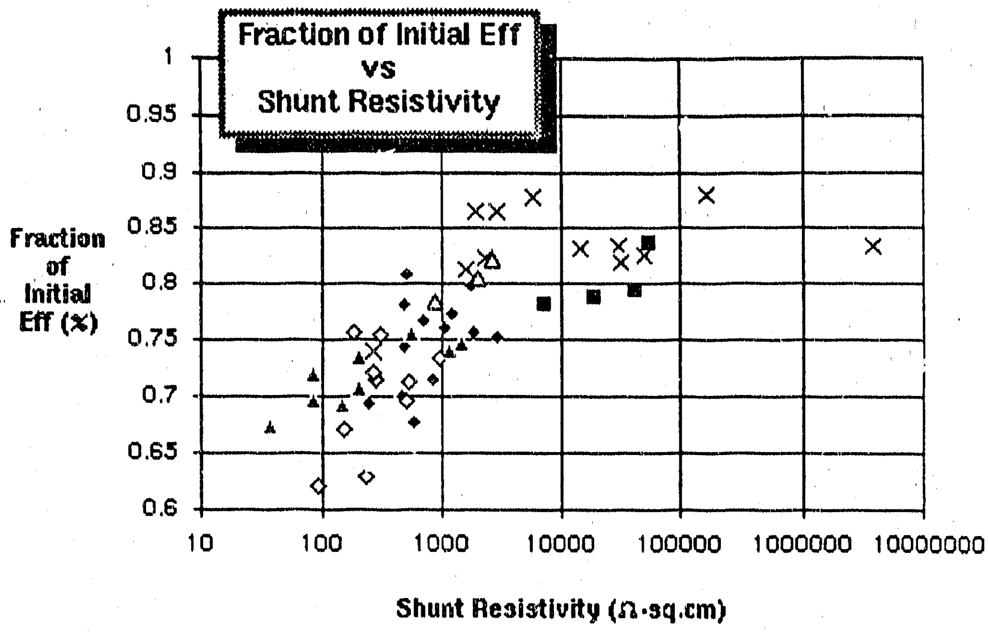

Fig. 2-6. Effect of shunting on TFS device performance. The different symbols on the chart represent different groups of devices.

effect then become controlling. For the state-of-the-art achieved in the Chatsworth research labs, the limits of these other mechanisms are on the order of 10-22% loss (100 mW/cm^2, 200+ hours, 50°C). Future advances in the materials and devices will further reduce these loss mechanisms.

Process control improvements are needed in order to improve the uniformity of ZnO. Figures 2-7 through 2-10 are maps of the performance of a 1×4 ft area that show the PV parameters of individual 1×4 cm test structure cells made on a 1×4 ft glass plate. The blank spaces in the figures imply no test, usually due to poor electrical connections between the cell and the test fixture. As shown in Fig. 2-7, the lower right corner of the 1×4 area has lower V_{oc}'s. Figure 2-8 also shows a band of low currents is along the right side. The best efficiency is, of course, where both the J_{sc} and fill factor are high (Fig. 2-10). The lowest efficiency is near the edges where both deposition non-uniformity and handling impact performance. In addition, a band of shunted devices is present to the right of center. The average efficiency of all cells is 9.5%, which is equivalent to a 32.8 watt 1×4 ft module.

The optimal TFS and front ZnO thicknesses are different for the semitransparent TFS module for tandem compared to stand-alone TFS

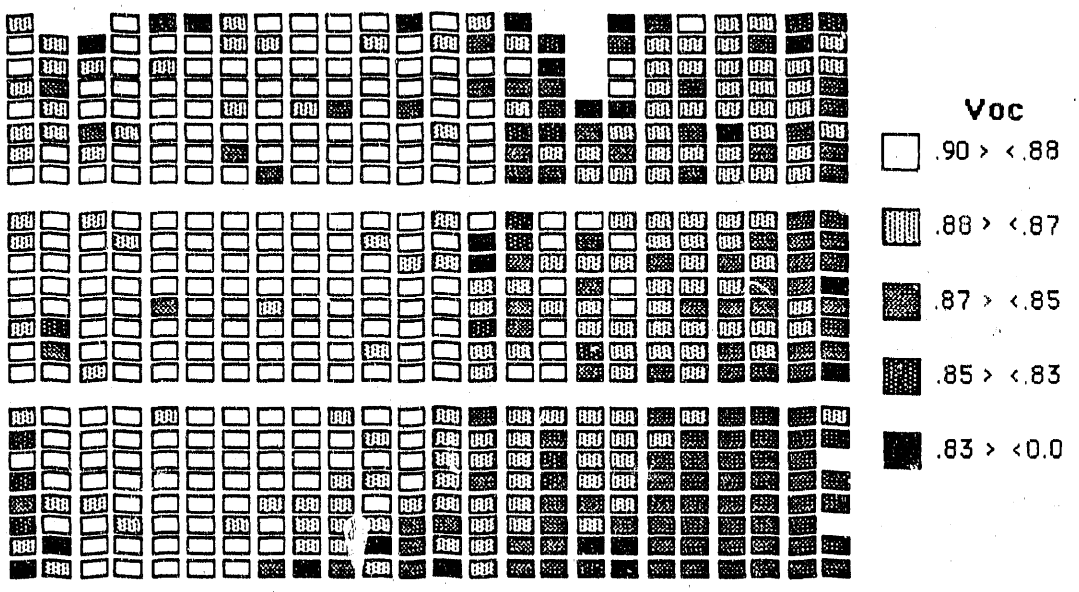

Fig. 2-7. Map of TFS V_{oc} (volts) performance.

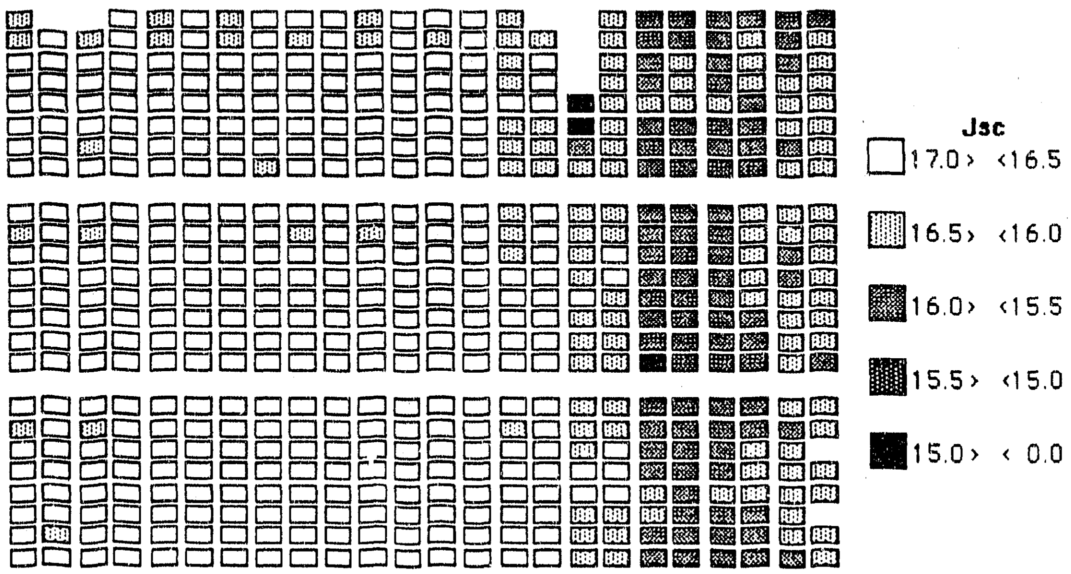

Fig. 2-8. Map of TFS J_{sc} (mA/cm^2) performance.

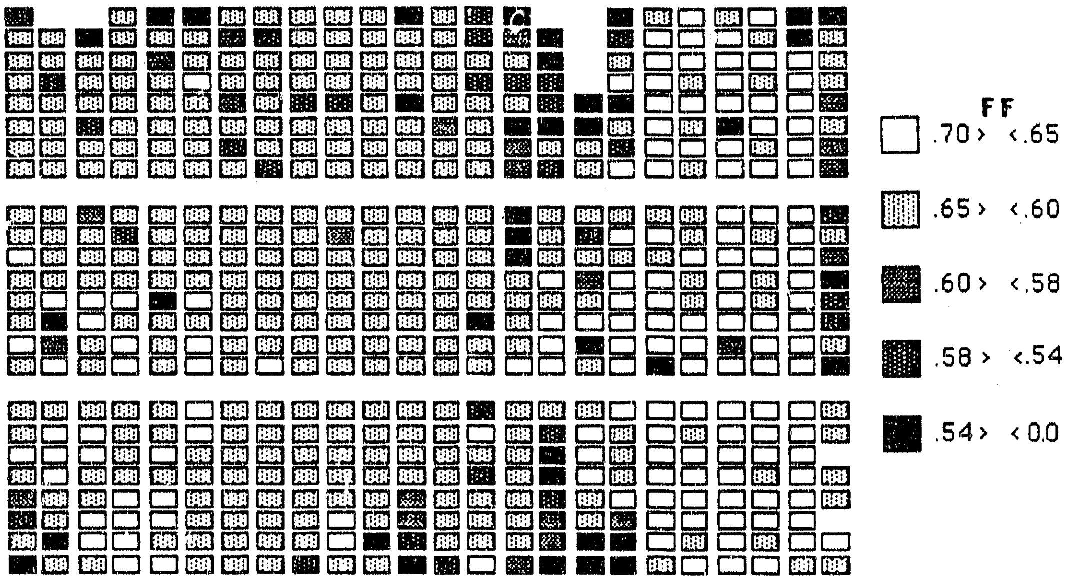

Fig. 2-9. Map of TFS fill factor performance.

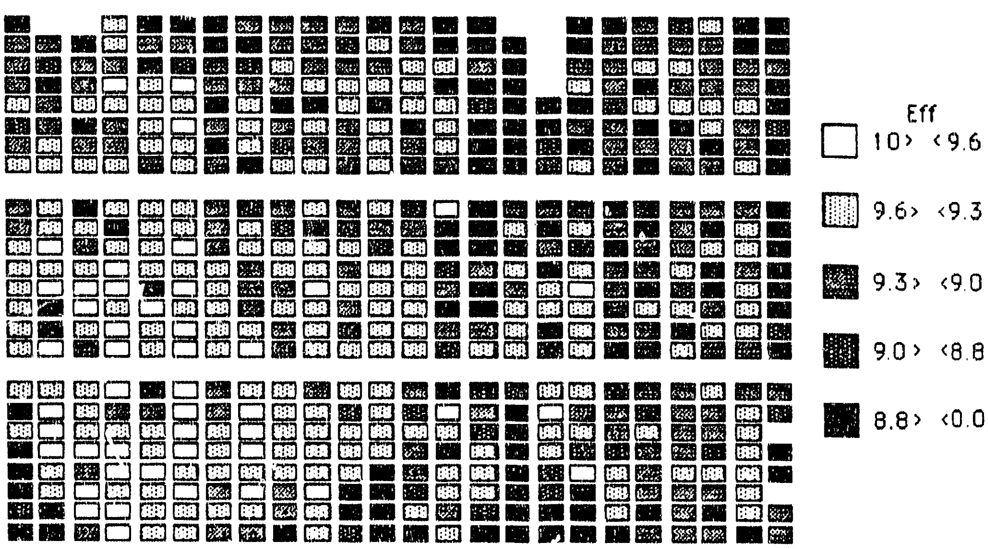

Fig. 2-10. Map of TFS efficiency performance.

modules. This difference is in part to take advantage of the high performance and stability of the CIS module. To study performance trade-offs, the ZnO layers and the TFS *i*-layer of a group of modules were made thinner (230-280 nm versus 350 nm) to increase their optical transmission. Part of the group also had half the standard doping of the ZnO to further improve transmission. Figures 2-11 and 2-12 plot module power and slope at V_{oc} as functions of front ZnO thickness. The ranges in ZnO thickness listed reflect the variations measured across the individual 1×4 ft modules. The slope at V_{oc} provides an indication of module series resistance as it impacts fill factor and thus power output. For the lower doped ZnO, the ZnO resistivity would be higher, resulting in higher ZnO sheet resistance which increases the overall module series resistance. This is reflected in the higher slopes at V_{oc} found in Fig. 2-12. For the standard doped ZnO, the ZnO contribution to module series resistance is reduced as reflected in the lower slopes at V_{oc}. This results in the higher module powers shown in Fig. 2-11.

The thinner TFS *i*-layers (230-280 nm) had lower module outputs (3-4 watts less) on average than standard (350 nm) modules. CIS modules filtered by these thin modules gave 1-2 watts more than those filtered by standard TFS modules. Thus, the combined initial power for the TFS/CIS tandem module is less using the thin TFS *i*-layer compared to the standard *i*-layer. But the stabilized tandem power output using the thin TFS *i*-layer may exceed that of the tandem module using the standard TFS *i*-layer, depending on the relative stability of the respective TFS *i*-layers. It is expected that the thinner TFS *i*-layer module will be more stable. Further work is necessary to address these issues.

2.4 TFS CELL AND MODULE PERFORMANCE

The particle control improvements installed in the Camarillo facility have increased the yielded power of 1×4 ft modules as demonstrated in Fig. 2-13. The average 1×4 ft TFS power output in February 1990 was 29.75 watts compared to 28.8 watts in August 1989. In addition, the distribution in module power was tighter in February.

The best white-backed 1×4 ft module fabricated in Camarillo generates 33.2 watts with a corresponding 8.4% aperture area efficiency as shown in Fig. 2-14. To evaluate the impact of scaling the module process from 1×1 ft to 1×4 ft, several 1×4 ft modules were cut into individual 1×1 ft module segments and the performances compared. Presently the 1×4 ft module efficiency averages 92% of the best 1×1 ft module piece cut from it. This suggests that the best 1×4 ft module above might produce a best 1×1 ft module efficiency of 9.1% (8.4%÷0.92), which compares well with the best 1×1 ft white-backed TFS module fabricated in Chatsworth with a 9.4% aperture area efficiency. The wider interconnects

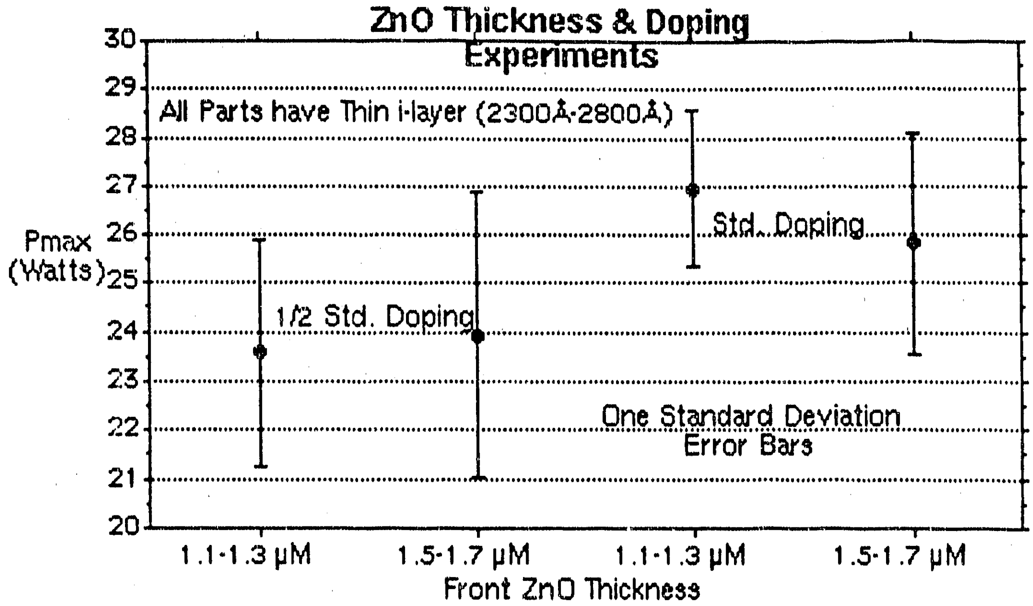

Fig. 2-11. Effect of ZnO thickness and doping on TFS submodule power.

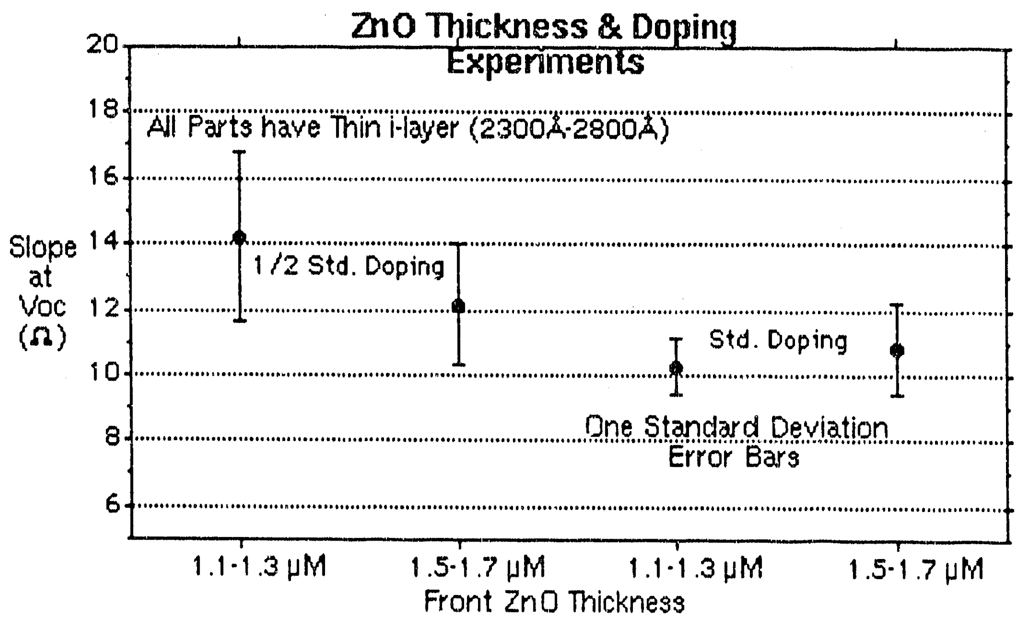

Fig. 2-12. Effect of ZnO thickness and doping on TFS V_{oc}.

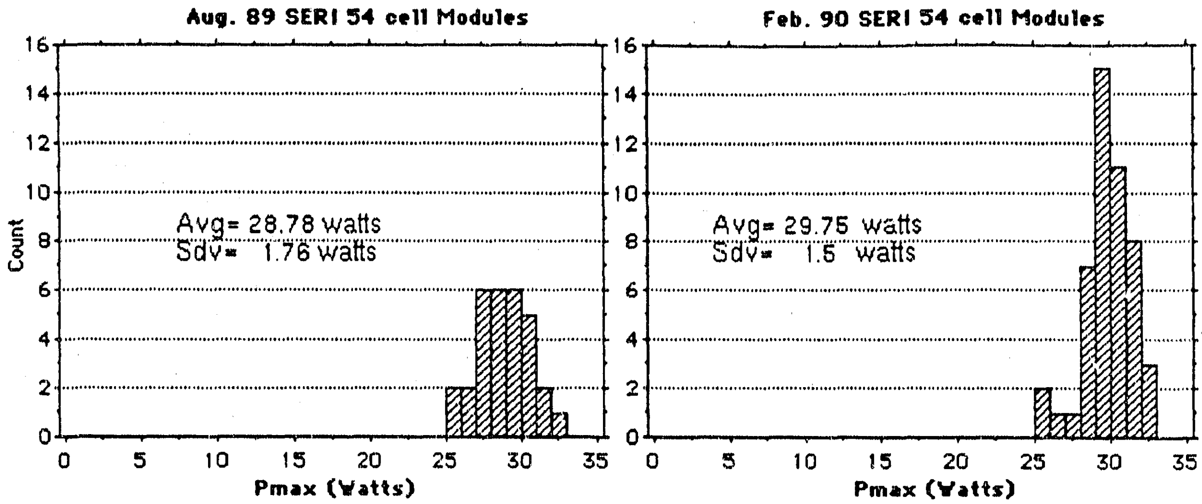

Fig. 2-13. Effect of particle control improvements on yield of TFS modules.

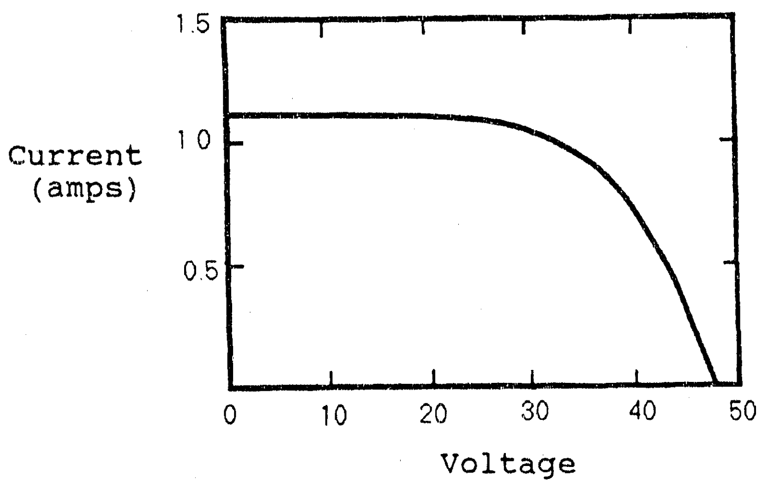

Aperture Area = 3970 cm^2
V_{oc} = 47.35 volts
I_{sc} = 1.14 amps
FF = 0.614
Eff = 8.4%
V_{mp} = 35.21 volts
I_{mp} = 943.5 mA
P_{max} = 33.2 watts

Fig. 2-14. Best 1×4 ft TFS module fabricated in Camarillo.

(0.046 cm) used for the present 1×4 ft TFS modules versus 0.013 cm for the best 1×1 ft TFS module accounts for the difference in the 1×1 ft efficiencies. This indicates that the basic TFS junction fabrication process has been adequately transferred from Chatsworth to large-area processing equipment in Camarillo.

In general, a comparison of the module cell V_{oc}, J_{sc}, and fill factor indicates that the largest gains to be made are in V_{oc} and fill factor. Continued reductions in junction shunting with improvements in particle control and better ZnO uniformity are expected to yield this improvement.

2.5 DISCUSSION

Emphasis during this period has been on the scaling of TFS module technology to 1×4 ft areas, resulting in demonstration of a 33.2 watt (8.4% aperture efficiency) back-reflector 54-cell module. Identifying and addressing several process sensitivities such as glass substrate qualitv and particulate control improved average module power, outdoor stability, and performance distributions. Further improvements such as ZnO uniformity, particulate control at the front ZnO patterning step, reduced electrical shunting, continued optimization of the layer thicknesses and doping, and narrower interconnects for the 1×4 ft modules will result in aperture efficiencies approaching 10%. Improved TFS junction quality, primarily through higher V_{oc}, will achieve module efficiencies exceeding 10%.

SECTION 3.0

TANDEM PROGRESS

3.1 TFS/CIS TANDEM CELL AND MODULE PERFORMANCE

Tandem modules are fabricated by laminating a semitransparent TFS module onto a CIS module (Fig. 3-1). The glass/glass laminate construction provides a rugged, environmentally durable package.

The TFS/CIS tandem cell and module performance results achieved during the contract are summarized in Tables 3-1 through 3-3. During Phase I, a 15.6% active area efficient TFS/CIS tandem cell was demonstrated using a 10.3% semitransparent TFS and a 12.4% efficient CIS cell. In addition, a 12.3% aperture area efficient, 843 cm^2 4-terminal TFS/CIS module was measured using a 7.7% efficient semitransparent TFS module and a 7.6% efficient CIS module. The TFS-filtered CIS module contributed 2.7% efficiency to the tandem output, which is 35% of its stand-alone performance. The filtered CIS module output is primarily defined by its lower short-circuit current, which is 37% of its unfiltered value. During Phase IIB, the 33.2 watt TFS module (discussed in Section 2.3) without the white back reflector measured 30.2 watts or 7.6% efficient. Placing a laminated 31.6 watt, 8.1% efficient CIS module underneath this TFS module, with an air gap between the two modules, produced 11.2 watts or 2.9% over a 3883 cm^2 aperture area. Thus, the 4-terminal tandem power output is 41.4 watts, translating to 10.5% aperture efficiency. The TFS-filtered to unfiltered CIS power ratio of 0.35 is dominated by a current ratio of 0.38.

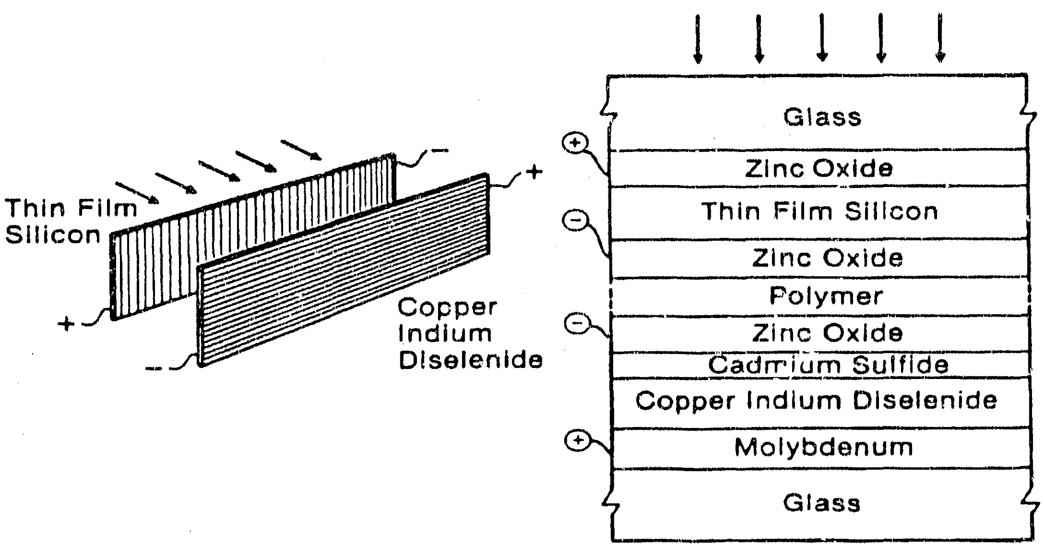

Fig. 3-1. TFS/CIS tandem module structure.

Table 3-1. 4-terminal tandem cell performance[a].

4 cm^2 Cell	Eff. (%)	J_{sc} (mA/cm^2)	V_{oc} (mV)	FF
Semitransparent TFS	10.3	16.4	871	0.72
Filtered CIS	5.3	17.9	432	0.68
Tandem	15.6			
Stand-Alone CIS	12.4	41.2	455	0.66

[a]Measured at ASTM air mass 1.5, global 100 mW/cm^2, 25°C.

Table 3-2. 1×1 ft tandem module performance[a].

30×30 cm Module	Power (W)	Area[b] (cm^2)	Eff. (%)	I_{sc} (mA)	V_{oc} (V)	FF
Semitransparent TFS	7.69	843	9.1	262	43.5	0.68
Filtered CIS	2.66	843	3.2	228	19.2	0.61
Tandem	10.35		12.3			
Stand-Alone CIS	7.62	844	9.0	611	21.2	0.59

[a]Measured at ASTM air mass 1.5, global 100 mW/cm^2, 25°C.
[b]Aperture area.

Table 3-3. 1×4 ft tandem module performance[a].

32×128 cm Module	Power (W)	Area[b] (cm^2)	Eff. (%)	I_{sc} (A)	V_{oc} (V)	FF
Semitransparent TFS	30.2	3970	7.6	1.03	47.2	0.62
Filtered CIS	11.2	3883	2.9	0.81	20.8	0.59
Tandem	41.4		10.5			
Stand-Alone CIS	31.6	3883	8.1	2.39	23.1	0.57

[a]Measured at ASTM air mass 1.5, global 100 mW/cm^2, 25°C.
[b]Aperture area.

3.2 LAMINATED AND FRAMED TFS/CIS TANDEM 1×4 FT MODULES

Five 1×4 ft TFS modules were selected for tandem fronts. Three had standard thickness *i*-layers (3500 Å) and two had thinner *i*-layers (2500 Å). The companion CIS modules ranged from 32 to 35 watts in stand-alone mode. As discussed in Section 2.3, the thinner *i*-layer TFS modules are more transparent and typically produce 3-4 watts less power themselves, but they allow the TFS-filtered CIS module to produce 1-2 watts more power.

Pre-lamination measurements were made with an air gap. Post-lamination measurements showed that less light was reflected back into the TFS and more was coupled into the CIS. Two of the CIS modules became open circuited after the tandem package was framed. Framing was done in a reaction injection mold (RIM). It is believed that the electrical connection between the external cable and the module bus ribbon became open-circuited during the RIM framing process.

I-V tests on the Spire LAPSS at SERI were in good agreement (within 1% for two of the modules) with Siemens Solar LAPSS measurements (Table 3-4). The three tandem modules delivered to SERI had maximum power between 35 and 36 watts. The close agreement between SERI and ARCO Solar measurements was established in Phase I.

Table 3-4. Measured power in watts of tandem modules.

Module ID	Module Layer	Siemens Solar Measurements Before Lamination	After Lamination	After Framing	SERI Measurements
1	TFS	27.10	25.80	25.40	
	CIS	9.25	10.20	0.0	open circuit
	Tandem	36.35	36.00	25.40	
2	TFS	26.90	25.80	25.30	
	CIS	8.54	10.10	8.79	open circuit later
	Tandem	35.44	35.90	34.09	
3	TFS	23.40	24.00	24.00	23.52
	CIS	10.40	11.70	12.20	11.50
	Tandem	33.80	35.70	36.20	35.02
4	TFS	24.30	23.40	23.60	24.12
	CIS	11.10	12.60	12.50	11.84
	Tandem	35.40	36.00	36.10	35.96
5	TFS	27.30	26.30	26.50	27.10
	CIS	9.30	9.90	8.84	7.95
	Tandem	36.60	36.20	35.34	35.05

3.3 DISCUSSION

The demonstration of the high efficiency TFS/CIS tandem concept has evolved during the contract from initial test cell structures to 1×1 ft modules to 1×4 ft modules. The larger size is comparable to conventional single crystal Si commercial modules and represents a high efficiency thin film power product. Several issues have been identified for further development. Laminated and RIM framed 1×4 ft 4-terminal TFS/CIS tandem modules have been delivered to SERI for evaluation.

The future performance of TFS/CIS tandem modules has been modeled. Tandem modules with 17.2% aperture-area efficiency generating 67 watts on an area of 3900 cm^2 are projected when junction efficiency and module fabrication goals are achieved (Table 3-5). In the tandem module stack, the semitransparent TFS module contributes 44.4 watts or 11.4% efficiency, and the CIS module contributes 22.6 watts or 5.8%. The stand-alone CIS module would generate 51.6 watts or 13.3%.

The model assumes a TFS optical filter factor (filtered-to-stand-alone CIS photocurrent ratio) of 0.46. The CIS module performance assumes a 14.1% junction efficiency already demonstrated on 3.5 cm^2 (see Section 1.2). The TFS module performance assumes 17.5 mA/cm^2 J_{sc}, 940 mV V_{oc}, and 8 Ω/cm^2 ZnO electrode sheet resistance. TFS cells with 12.0% efficiency, 17.7 mA/cm^2 J_{sc}, and 965 V_{oc} [1] and with 11.7% efficiency, 18.1 mA/cm^2 J_{sc}, and 915 V_{oc} [2] have been reported.

Table 3-5. Projected TFS/CIS tandem module performance.

53-Cell Module	Power (W)	Area (cm^2)	Eff (%)	I_{sc} (A)	V_{oc} (V)	FF
Semitransparent TFS	44.4	3890	11.4	1.22	49.8	0.73
Filtered CIS	22.6	3890	5.8	1.31	25.2	0.68
Tandem	67.0		17.2			
Unfiltered CIS	51.6	3890	13.3	2.85	26.9	0.67

[a] ASTM air mass 1.5, global 100 mW/cm^2, 25°C.
[b] Aperture area.

SECTION 4.0

REFERENCES

Summary

1. W. Bottenberg, K. Mitchell, D. Morel. Phase I Task B Technical Progress Report, Contract ZB-7-06003-3 (1988).

2. C. Eberspacher, J. Ermer, D. Tanner. K.W. Mitchell, Project Director. Phase IIA Task B Technical Progress Report, Contract ZB-7-06003-3 (1989).

Section 1.0: CIS Progress

1. W. Bottenberg, K. Mitchell, D. Morel. Phase I Task B Technical Progress Report, Contract ZB-7-06003-3 (1988).

2. C. Eberspacher, J. Ermer, D. Tanner. K.W. Mitchell, Project Director. Phase IIA Task B Technical Progress Report, Contract ZB-7-06003-3 (1989).

3. Personal communication with L. Mrig, Solar Energy Research Institute, Golden, CO. (1989)

4. K.W. Mitchell et al., *Proc. 8th European Photovoltaic Solar Energy Conf.*, Florence, Italy, pp. 1578-1582 (1988).

5. ASTM Standard E892, "Terrestrial Solar Spectral Irradiance Tables at Air Mass 1.5 for a 37 deg. Tilted Surface", American Society for Testing and Materials, Philadelphia, PA. (1985).

6. J.R. Tuttle, R. Noufi, R.G. Dhere, *19th IEEE Photovoltaic Specialists Conf.*, pp. 1494-1495 (1987).

7. K.W. Mitchell, H.I. Liu, *20th IEEE Photovoltaic Specialists Conf.*, pp. 1461-1468 (1988).

8. W. Chesarek, A. Mason, K. Mitchell, L. Fabick, *19th IEEE Photovoltaic Specialists Conf.*, pp. 791-794 (1987).

9. W. Chesarek, K. Mitchell, A. Mason, L. Fabick, *Solar Cells*, 24, pp. 263-270 (1988).

10. M. Nicolet, *Investigations of $CuInSe_2$ Thin Films and Contacts*, Semiannual Report, SERI Contract # XB-8-07133-1, May 5, 1989.

11. K. Mitchell, C. Eberspacher, J. Ermer, D. Pier, *20th IEEE Photovoltaic Specialists Conf.*, pp. 1384-1389 (1988).

Section 2.0: TFS Progress

1. W. Bottenberg, K. Mitchell, D. Morel. Phase I Task B Technical Progress Report, Contract ZB-7-06003-3 (1988).

2. C. Eberspacher, J. Ermer, D. Tanner. K.W. Mitchell, Project Director. Phase IIA Task B Technical Progress Report, Contract ZB-7-06003-3 (1989).

3. K.W. Mitchell, C. Eberspacher, J. Ermer, K. Pauls, D. Pier, D. Tanner, Proc. DOE/SERI Amorphous Silicon Subcontractors' Review Meeting, Golden, CO, June 19-20, 1989.

4. K.W. Mitchell, Proc. DOE/SERI Amorphous Silicon Subcontractors' Review Meeting, Golden, CO, June 19-20, 1989.

Section 3.0: Tandem Progress

1. Y. Hattori, D. Kruangam, T. Toyama, H. Odamoto, Y. Hamakawa. *Proc. 3rd International Photovoltaic Science and Engineering Conf.*, Tokyo, pp. 171-174 (1987).

2. M. Konagi. *Proc. 3rd International Photovoltaic Science and Engineering Conf.*, Tokyo, pp. 15-20 (1987).

SECTION 5.0

PAPERS PUBLISHED DURING PHASE IIB

The following papers and reports have been produced under SERI Subcontract ZB-7-06003-3, titled "Research on Stable, High Efficiency, Large-Area, Amorphous Silicon Based Submodules."

"Recent Progress in Large Area $CuInSe_2$ Submodules." J. Ermer, C. Fredric, K. Pauls, D. Pier, K. Mitchell, C. Eberspacher, ASI; K. Kushiya, Showa ARCO Solar KK. *Proceedings, PVSEC-4, 4th International Photovoltaic Science and Engineering Conference*, Sydney, Australia, Feb. 14-17, 1989, pp. 475-480. Inst. of Radio and Electronics Engineers, Australia (1989).

"Single and Tandem Junction $CuInSe_2$ Technology." K. Mitchell, C. Eberspacher, J. Ermer, K. Pauls, D. Pier, D. Tanner. *Proceedings, PVSEC-4, 4th International Photovoltaic Science and Engineering Conference*, Sydney, Australia, Feb. 14-17, 1989, pp. 889-896. Inst. of Radio and Electronics Engineers, Australia (1989).

"Research on Amorphous Silicon-Based Thin Film Photovoltaic Devices, Task B." Technical Progress Report for the period September 1, 1988 through February 28, 1989. C. Eberspacher, J. Ermer, D. Tanner, K. Mitchell.

"Status of $CuInSe_2$ Photovoltaic Technology." K. Mitchell, C. Eberspacher, K. Pauls. International Symposium on Uses of Selenium and Tellurium, Banff, Alberta, Canada, May 8, 1989.

"Progress on High Efficiency Thin Film Cells and Submodules." Kim W. Mitchell, C. Eberspacher, J. Ermer, K. Pauls, D. Pier, D. Tanner. SERI 9th Photovoltaic Advanced Research and Development Project Review Meeting, Lakewood, CO, May 24-26, 1989, and *Solar Cells*, Vol. 27, pp. 69-76 (1989).

"High Efficiency Si:H/$CuInSe_2$ Thin Film Cells and Submodules." Kim W. Mitchell, C. Eberspacher, J. Ermer, K. Pauls, D. Pier, D. Tanner. DOE/SERI Amorphous Silicon Subcontractors' Review Meeting, Golden, CO, June 19-20, 1989.

"Perspectives on Thin Film Module Development." Kim W. Mitchell. DOE/SERI Amorphous Silicon Subcontractors' Review Meeting, Golden, CO, June 19-20, 1989.

"Status of $CuInSe_2$ Cells and Submodules." Kim W. Mitchell, C. Eberspacher, J. Ermer, K. Pauls, D. Pier. *Proceedings of the Polycrystalline Thin Film Program Meeting*, Lakewood, CO, Aug.

16-18, 1989, Technical Report SERI/CP-211-3550, pp. 199-205. Solar Energy Research Institute, Golden, CO (1989).

"Copper Indium Diselenide: Towards 20% Efficiency." Kim W. Mitchell. *Commission of the European Communities 9th E.C. Photovoltaic Solar Energy Conference,* Freiburg, Federal Republic of Germany, Sept. 25-29, 1989, pp. 292-293. Kluwer Academic Publishers, Dordrecht, Holland (1989).

"Research on Stable, High Efficiency, Large-Area, Amorphous Silicon Based Submodules." Kim W. Mitchell. Prepared for Office of Program Analysis Photovoltaic Program Review, Nov. 14-16, 1989.

"Fundamental Mechanisms Controlling $CuInSe_2$ Solar Cells and Module Performance." Kim W. Mitchell. Prepared for Office of Program Analysis Photovoltaic Program Review, Nov. 14-16, 1989.

"Research on Amorphous Silicon Based Thin Film Photovoltaic Devices." K.W. Mitchell, C. Eberspacher, D. Tanner, D. Willett. *Annual Report Photovoltaic Program Branch FY 1989*, Technical Report SERI/PR-211-3483, Solar Energy Research Institute, Golden, CO.

"$CuInSe_2$ Cells and Modules." K.W. Mitchell, C. Eberspacher, J. Ermer, K. Pauls, D. Pier. Special issue *Transactions on Electron Devices on Photovoltaic Materials, Devices, and Technologies*, Vol. 37, No. 2, pp. 410-417.

"Advances in Large Area $CuInSe_2$ Thin Film Modules." J. Ermer, C. Fredric, J. Hummel, C. Jensen, D. Pier, D. Tarrant, K. Mitchell. *Proc. 21st IEEE Photovoltaic Specialists Conf.*, May 21-25, 1990 (to be published).

"Advances in Large Area Si:H Thin Film Modules." D.R. Willett, S.A. Vasquez, D.P. Tanner. *Proc. 21st IEEE Photovoltaic Specialists Conf.*, May 21-25, 1990 (to be published).

"41.5 Watt, 10.5% Si:H/$CuInSe_2$ Tandem Thin Film Modules." K.W. Mitchell, D. Willett, C. Eberspacher, J. Ermer, D. Pier, K. Pauls. *Proc. 21st IEEE Photovoltaic Specialists Conf.*, May 21-25, 1990 (to be published).

"Thin Film Solar Cells -- Devices, Materials and Fabrication." Kim Mitchell. Tutorial at the 21st IEEE Photovoltaic Specialists Conf., May 21-25, 1990.

Document Control Page	1. SERI Report No. SERI/TP-211-3967	2. NTIS Accession No. DE91002115	3. Recipient's Accession No.
4. Title and Subtitle Research on Stable, High-Efficiency, Large-Area Amorphous Silicon Based Modules - Task B			5. Publication Date October 1990
			6.
7. Author(s) K. W. Mitchell, D. R. Willet			8. Performing Organization Rept. No.
9. Performing Organization Name and Address Siemens Solar Industries 4650 Adohr Lane Camarillo, CA 93010			10. Project/Task/Work Unit No. PV040201
			11. Contract (C) or Grant (G) No. (C) ZB-7-06003-3 (G)
12. Sponsoring Organization Name and Address Solar Energy Research Institute 1617 Cole Blvd. Golden, CO 80401			13. Type of Report & Period Covered Technical report
			14.

15. Supplementary Notes
SERI technical monitor: W. Luft

16. Abstract (Limit: 200 words)

This report documents progress in developing a stable, high-efficiency, four-terminal hybrid tandem module. The module consists of a semi-transparent, thin-film silicon:hydrogen alloy (TFS) top circuit and a copper indium diselenide ($CuInSe_2$) bottom circuit. Film deposition and patterning processes were successfully extended to 0.4-m^2 substrates. A 33.2-W (8.4% efficient) module with a 3970-cm^2 aperture area and a white back reflector was demonstrated; without the back reflector, the module produced 30.2 W (7.6% efficient). Placing a laminated, 31.6-W, 8.1%-efficient $CuInSe_2$ module underneath this TFS module, with an air gap between the two, produces 11.2 W (2.9% efficient) over a 3883-cm^2 aperture area. Therefore, the four-terminal tandem power output is 41.4 W, translating to a 10.5% aperture-area efficiency. Subsequently, a 37.8-W (9.7% aperture-area efficiency) $CuInSe_2$ module was demonstrated with a 3905-cm^2 aperture area. Future performances of single-junction and tandem modules of this size were modeled, and predicted power outputs exceed 50 W (13% efficient) for $CuInSe_2$ and 65 W (17% efficient) for TFS/$CuInSe_2$ tandem modules.

17. Document Analysis
a. Descriptors
photovoltaics ; solar cells ; amorphous silicon ; large area ; modules ; high efficiency

b. Identifiers/Open-Ended Terms

c. UC Categories
271

18. Availability Statement National Technical Information Service U.S. Department of Commerce 5285 Port Royal Road Springfield, VA 22161	19. No. of Pages 39
	20. Price A03

Form No. 0069E (6-30-87)

END

DATE FILMED

02 / 08 / 91